Check for updates

ADVANCED INTELLIGENT SYSTEMS
Open Access
www.advintellsyst.com

Origami-Inspired Modular Electro-Ribbon Actuator for Multi-Degrees of Freedom Motion

*Ningzhe Hou, Jian Wen, Yuhan Pan, and Majid Taghavi**

Origami robots, inspired by an ancient form of paper folding art, are capable of achieving high displacement in a lightweight and compact design that conventional robots can hardly attain. It, however, remains a challenge to drive origami robots with in situ active materials that imply minimal added mass and complexity and can be easily controlled to achieve multiple actuation modalities. Herein, inspired by the Twisted Tower origami structure, dielectrophoretic liquid zipping actuation concept is employed to develop a modular architecture, capable of achieving complicated motions with multiple degrees of freedom (DoF). The experimental results show a maximum of 3.9 degrees tilting per layer toward any desired direction, a 56.1% contraction of the original length, and 5.4 degrees twisting per layer. Each layer can generate a maximum contractile force of 1.03 N with a maximum 64.7% power efficiency and 2.775 W kg^{-1} power-to-weight ratio. A modified heterochiral arrangement of this modular actuator is proposed to enhance controllability across various movement modes. Its use in robotic-wrist-like actuation has been demonstrated, highlighting its significant potential for integration into soft robotic multi-DoF structures, such as continuum arms.

1. Introduction

Active structures to incorporate movement in multiple degrees of freedom (DoF) have always posed a significant challenge in both structural and material design. Conventionally, achieving multimodal motion in a single structure, including bending, twisting, and contraction/expansion, necessitates intricate design approaches with the integration of multiple actuators.[1] The human wrist, for example, showcases 2-DoF motion, allowing for flexion, extension, radial deviation, ulnar deviation, in addition to a third DoF motion achieved through forearm pronation, and supination. Mimicking such complex movements in prosthetic wrist designs is a considerable challenge.[2] Achieving the same level of flexibility as the human wrist necessitates a complicated mechanical design equipped with several motors. However, the complexity of such designs typically results in heavy wearables and prosthetics with decreased robustness, especially under intensive use. In light of these challenges, innovative structural approaches have received interest to develop multimodal movement.

Origami-inspired designs, recognized for their enabling multimodal actuation,[3,4] present significant potential in applications demanding diverse range of motion capabilities. The term "origami" means "paper folding" in Japanese and is an ancient form of art that can be traced back to 1000 years ago.[5] It has been recently found that origami is way more than simply folding paper to imitate objects or animals. Many of the naturally evolved organic structures, such as the leaf and the wing of the insects, and even the folding of chains of amino acids in protein,[6] show remarkably high similarities to the origami patterns. The concept of origami for combining the compliant and rigid structure on a single piece of material also inspires the new generation of robotic material design and manufacturing. This exploration aims to leverage metamaterial properties to equip robots with increased DoF and flexibility. For instance, many origami structures involve the repeated use of a single pattern, which could provide inspirations to the design of modular and reconfigurable robots.[7] A wide range of soft robotics designs inspired by the origami structure have already shown the potential of the combination of origami and robotics.[8,9]

One of the main challenges in designing the origami robot is the actuation. Distinct from the traditional robot designs, the higher DoF in origami robots enabled by the recursive folding patterns makes them particularly difficult to actuate by motors. A variety of different actuation method have been designed to move the origami robot, which can be classified as active and passive structures. Active structures imply that the structure is capable of actuating itself without any external actuators whereas passive structures need external actuators to move them.

Passive structures are the most widely used method to drive origami robots, which mainly consists of motor-driven, magnet-driven, fluid-driven, and thread-driven. Mori,[7] a reconfigurable modular robot inspired by the origami structure, is a good example of incorporating traditional motors into an origami structure. Each of the origami elements consists of three micromotors, which enable multiple configurations and motion of the robot.

N. Hou, J. Wen, Y. Pan, M. Taghavi
Department of Bioengineering
Imperial College London
86 Wood Ln, London W12 0BZ, UK
E-mail: m.taghavi@imperial.ac.uk

The ORCID identification number(s) for the author(s) of this article can be found under https://doi.org/10.1002/aisy.202300738.

© 2024 The Authors. Advanced Intelligent Systems published by Wiley-VCH GmbH. This is an open access article under the terms of the Creative Commons Attribution License, which permits use, distribution and reproduction in any medium, provided the original work is properly cited.

DOI: 10.1002/aisy.202300738

26404567, 2024, 6, Downloaded from https://advanced.onlinelibrary.wiley.com/doi/10.1002/aisy.202300738 by Imperial College London, Wiley Online Library on [23/06/2025]. See the Terms and Conditions (https://onlinelibrary.wiley.com/terms-and-conditions) on Wiley Online Library for rules of use; OA articles are governed by the applicable Creative Commons License

Magnetic force is also an innovative method to drive the origami robots with a high mechanical response speed to the change in magnetic field,[10–12] but the controllability of the robot would bring further challenges in real-world applications. An intriguing design has been implemented, which utilizes a four-unit Kresling Origami structure.[13] This structure is augmented by distributed magnetic actuation and a segmented design, which together significantly improve its controllability. The fluid-driven is the most commonly used actuation for origami robots, the origami pattern is usually incorporated with sealed chambers, and the actuation is achieved by pressurizing[14,15] or vacuuming[16,17] the chamber. The fabrication of complicated Origami patterns can be easily achieved by mold casting[14] with silicon or 3D printing.[15] However, the source of the pressure is an obstacle to applying fluid-driven robots in many scenarios. In some of the designs, more than 45 kPa of required pressure make it challenging to actuate by a compact device.[18] Thread or tendon-driven origami structure[19,20] offers compliant solution to close the hinges but is still limited by the use of electrical servo or stepper motors.

In contrast, active structures offer an efficient approach to drive origami robots with minimal use of materials and complexity. Current solutions are primarily driven by shape-memory alloy (SMA), shape-memory polymer (SMP), and electrostatic force. The SMA and SMP origami structure enables programming the material into a desired shape. The material reverts to its originally programmed shape under certain conditions, such as exposure to high temperature or light. This feature can be combined with the 2D to 3D origami structures to design new generation medical artery implants.[21] However, the actuation is typically nonreversible, meaning that when the actuation condition is removed, the material returns to the seemingly plastically deformed state but will not deform without external force and remain in the programmed shape.[22] The power efficiency is extremely low for the SMA and SMPs, typically measuring between 1.08 and 1.32% for the SMPs.[23] The electrostatic force holds promise as the most potential method for the implementation as variable capacitor to actuate the origami structures. The power efficiency of the electrostatic actuators can reach as high as 70%.[24] Additional advantages such as microsecond-level fast response speed, high resilience, and an actuation strain exceeding 300%[23] further establish electrostatic actuators as an ideal choice to actuate the origami robot in various applications. Most importantly, electrostatic force can be solely controlled by adjusting voltage, which is ideal in many applications that require a compact control design. However, the electrostatic attraction force between two oppositely charged electrodes is inversely proportional to the square of the distance between the electrodes and thus rapidly decreases as the distance between the electrode increases. This limitation restricts the use of the electrostatic force between separated electrodes in microscale systems. The dielectrophoretic liquid zipping (DLZ) principle,[24] on the other hand, offers a solution to use this force on a larger scale, potentially amplifying the electrostatic force by 120 folds. In DLZ, two insulated electrodes are clamped together[24,25] at one end, generating a focused electric field at the hinge which enables the electrodes to attract each other and close, similar to a zipper. Adding a bead of high-breakdown-strength dielectric liquid at the hinge allows for sustaining the high electric field generated at the hinge, which moves along the electrodes when zips.[24] Other intrinsic characteristics of the DLZ concept that makes it attractive for driving origami structure are self-locking[26] and self-sensing.[27] The former implies that the actuator can maintain its closed position with minimum power consumption, potentially increasing the overall power efficiency of the actuator. Reading the capacitance variation between the electrodes provides the necessary information to detect the position of the actuation, and therefore, this self-sensing feature eliminates the need to integrate additional components for closed-loop control of the actuators.

Here, drawing inspiration from an origami structure, we develop Origami Zipping (OriZip), a compliant modular origami unit based on the DLZ principle. OriZip enables us to develop complicated repetitive structures that exhibits multi-DoF motion capability, including tilting along the x- and y-axis, shortening along the z-axis, and twisting along the z-axis. By stacking multiple layers of OriZip actuators in either similar or opposite orientations, various movement modalities are achievable, when each OriZip is controlled through adjusting its input voltage.

2. Design and Methods

We gain inspiration from the "Twisted Tower," a modular origami art designed by Mihoko Tachibana[28] as shown in **Figure 1**A. The design is scalable to any desired length by interconnecting multiple identical layers. Each layer is capable of four DoF motion, including tilting along the x- and y-axis, shortening along the z-axis to the small thickness of the layered papers, and twisting along the z-axis. In the Twisted Tower design, twisting occurs simultaneously with tilting and shortening at each layer. By stacking multiple layers in either heterochiral or homochiral configurations, we can achieve controlled overall twisting or tilting in the structure. Our design incorporates the DLZ actuation principle into the modified Twisted Tower modular origami structure. As shown in Figure 1D and Video S1, Supporting Information, when voltage is applied to the actuator, the electrostatic force generated at the hinge overcomes the elastic energy stored in the curved structure. This leads to a gradual collapse of the structure. Conversely, when the voltage is turned OFF, the actuator quickly rebounds to its original form, driven by the release of stored elastic energy.

2.1. Analysis Based on a 2D Paper Folding

Each layer of the Twisted Tower consists of eight identical regular frustum-shaped elements, called Twisted Tower building block. Each building block is formed by four bottom-connected trapezoids (**Figure 2**A), where each of the bottom-connected trapezoids shares one trapezoid with the neighboring building block, and each of them is folded by a single piece of paper. By unfolding the bottom-connected trapezoid structure, the geometrical relationships of the Twisted Tower can be analyzed based on the folding hinges.

As shown in Figure 2A, each paper is a rectangle with a side length ratio of 1:2 while the height of each trapezoid is half of the shorter side length, and the bottom has the relationship of 0.59s

 © 2024 The Authors. Advanced Intelligent Systems published by Wiley-VCH GmbH

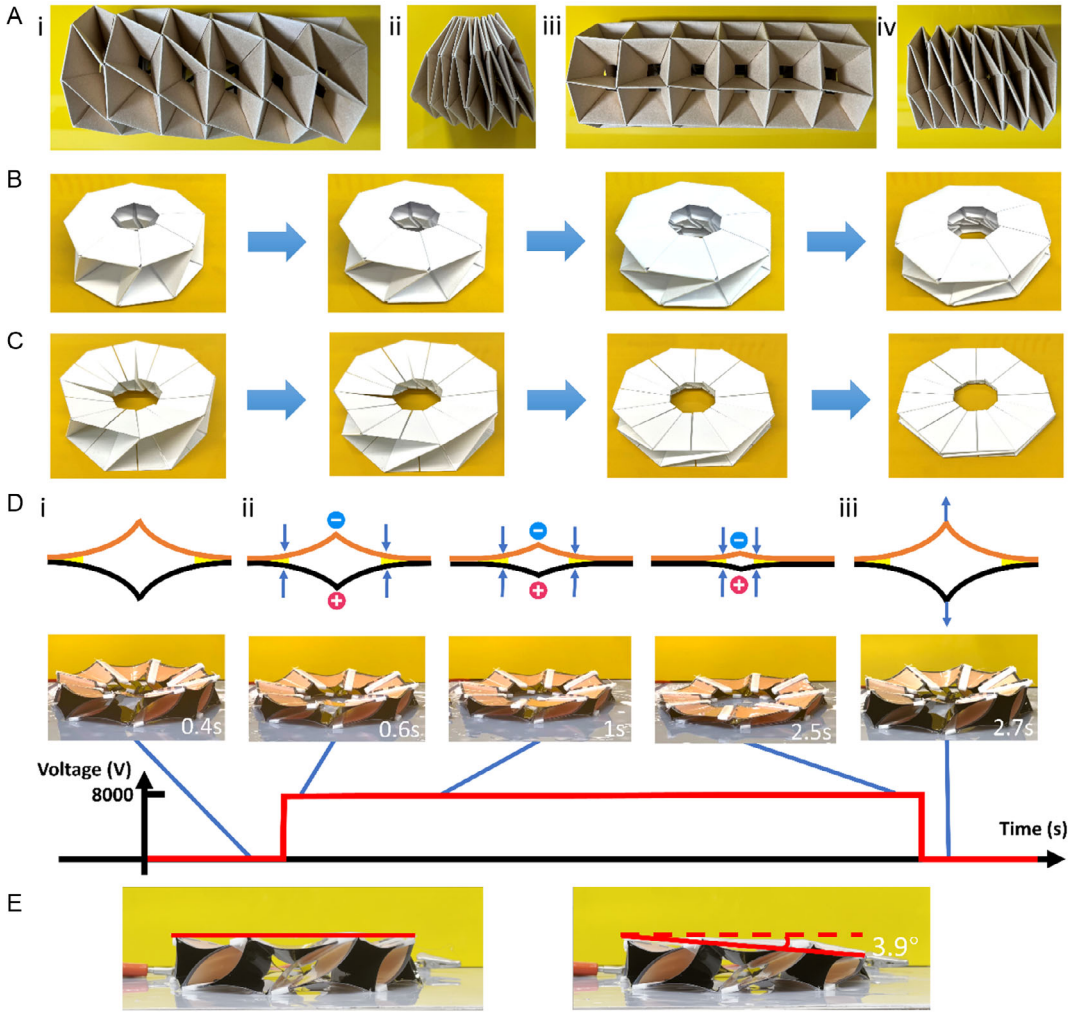


Figure 1. The electrozipping actuator inspired by the "Twisted Tower" Origami structure. A) Photos showing the twisted i), tilted ii), fully opened iii), and almost collapsed iv) states of the Twisted Tower. B) The single-layered origami paper-folded Twisted Tower. C) The modular structure of the Twisted Tower, composing eight geometric building block models. D) Single OriZip module actuation mechanism, and shortening and twisting motion of a single layer of the Twisted Tower along the *z*-axis with an indication of the corresponding actuation voltage. i) In the relaxing state, with no voltage applied, the dielectric liquid remains at the zipping hinge due to surface tension. ii) Application of voltage across the top and bottom electrodes induces electrostatic contracting force at the hinge, amplified by the dielectric liquid, initiating the closing motion of the OriZip module. In this closing state, the dielectric liquid migrates along the insulators and remains at the hinge due to dielectrophoresis. iii) Voltage removal allows the OriZip module to rebound to its original state via elastic energy recovery, with most of the dielectric liquid returning to the hinge, preparing the module for subsequent actuation. E) Illustration of the tilting motion of the actuator.

with the shorter side length *s*. The base angle at the longer base of the trapezoid is 67.5°, which is half of the interior angle of a regular octagon 135°. This implies that when one layer of eight building blocks, forming a circular pattern, is fully collapsed onto each other, they will collectively form a 2D regular octagon (Figure 2B). It is based on an assumption that the paper possesses negligible thickness, contributing to the precise geometric alignment. A geometric model made with plastic film and polyvinyl chloride (PVC) tape (Figure 2A, top right) is created based on the geometric relationships obtained from the folding hinge analysis to verify the result.

Based on the geometric relationships verified by the model, OriZip module is designed by integrating the DLZ actuation principle to actively control the folding. The electrostatic force between two conductive electrodes would exponentially decrease as the distance becomes larger. Moreover, the DLZ could only provide the amplified contraction force, but the repulsive force is insignificant. Active control of the OriZip unit would also require the repulsive force to restore the original shape after the active actuation is removed. Hence, a curvature with a 25 mm radius is applied on each of the trapezoids to restore the original shape of OriZip module by releasing the stored elastic energy when the actuation is removed. The curved design of our structure plays a crucial role in minimizing the angle at the prezipping hinges, where the two electrodes make contact. This reduced angle is crucial as it maximizes the zipping force, thereby enhancing the efficiency and effectiveness of the actuator's movement.

© 2024 The Authors. Advanced Intelligent Systems published by Wiley-VCH GmbH

26404567, 2024, 6, Downloaded from https://advanced.onlinelibrary.wiley.com/doi/10.1002/aisy.202300738 by Imperial College London, Wiley Online Library on [23/06/2025]. See the Terms and Conditions (https://onlinelibrary.wiley.com/terms-and-conditions) on Wiley Online Library for rules of use; OA articles are governed by the applicable Creative Commons License

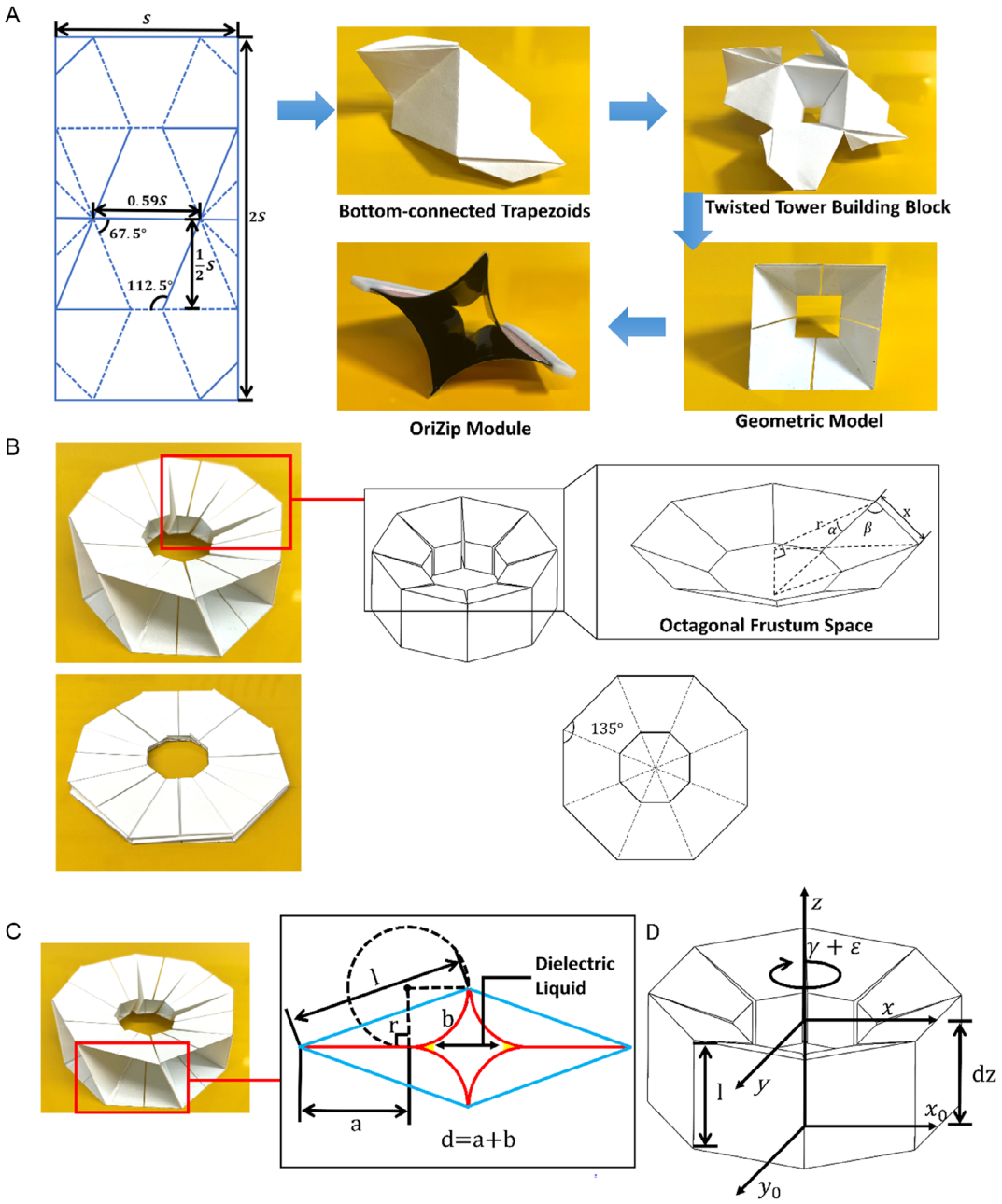


Figure 2. Geometric and kinematic analysis of the actuator. A) Evolution of the OriZip module: a single piece of paper is folded into two bottom-connected trapezoids, and four pairs of bottom-connected trapezoids form a Twisted Tower building block, where its building block informs the development of the OriZip Module. B) Analysis of the interval angle between neighboring Twisted Tower building blocks. C) Illustration of the relationship between the side length of OriZip, percentage of zipping, and the curved length. D) The illustration of the kinematic model based on the screw motion.

2.2. The Interval Angle Between the OriZip Modules

In the geometric model, there is always an interval between the Twisted Tower building block, which would create a certain level of instability and unpredictability for controlling the whole structure. The analysis is made geometrically on the cause of the interval angles between the building block. The fundamental key to achieving a full collapse of the layer lies in the square frustum shape of each building block, but square frustum shape also results in the formation of octagonal frustum spaces at the top and bottom when the model is not collapsed, as shown in Figure 2B. The relationship between the slant angle of the frustum α and the base angle of each trapezoid that forms the frustum β can be estimated by

$$\beta = arcos\left(\frac{x}{2r}\cos(\alpha)\right) \tag{1}$$

© 2024 The Authors. Advanced Intelligent Systems published by Wiley-VCH GmbH

26404567, 2024, 6, Downloaded from https://advanced.onlinelibrary.wiley.com/doi/10.1002/aisy.202300738 by Imperial College London, Wiley Online Library on [23/06/2025]. See the Terms and Conditions (https://onlinelibrary.wiley.com/terms-and-conditions) on Wiley Online Library for rules of use; OA articles are governed by the applicable Creative Commons License

26404567, 2024, 6, Downloaded from https://advanced.onlinelibrary.wiley.com/doi/10.1002/aisy.202300738 by Imperial College London, Wiley Online Library on [23/06/2025]. See the Terms and Conditions (https://onlinelibrary.wiley.com/terms-and-conditions) on Wiley Online Library for rules of use; OA articles are governed by the applicable Creative Commons License

where r represents the distance from the angle to the centroid of the octagon and x is the base length of the octagon. The fixed ration $\frac{x}{2r} = \cos\left(\frac{135^\circ}{2}\right)$ is derived because the bottom of the frustum forms a regular 2D octagon with an interior angle of 135°. As a result, each of the angles (β) is calculated to be 69.3°, which means there will be an angle of 3.6° at each of the neighboring building block resulting from the difference between the 2D octagon's 135° interior angle and the octagonal frustum's 138.6° (2β) 3D interior angle. These angles sum up to a total of 28.7°. Hence, the presence of this interval is an inherent feature of the Twisted Tower structure, and in fact, it is an important feature to ensure the full collapse of each layer.

2.3. The Kinematics of the Origami Structure

The motion of each layer involves simultaneous twisting and translation along the z-axis. The kinematics of such motion can be derived from the screw motion.[20] Unlike the paper folding version, which can collapse in two directions, the requirement of a prezipping hinge limits the twisting direction of each layer to one direction, and the prezipping clamping has created a certain rotation angle. The geometric relationships restrict the rotation to $\gamma + \varepsilon \leq \frac{\pi}{4} - \theta$ or $-\frac{\pi}{4} + \theta \leq \gamma + \varepsilon$, where the γ and ε denote the initial twisted angle created by the prezipping and the actuation twisted angle, respectively, and the θ is the angle caused by the paper thickness. Another difference between the paper folding version and the electrozipping actuator is the curvature for the zipping angle and the restoration of elastic energy. It implies that the side length of the parallelogram formed by each OriZip unit is no longer constant.

As shown in Figure 2C,D, a geometric model is proposed, and the side length of the parallelogram formed by the actuator can be derived as

$$l = \sqrt{(kd)^2 + \left(2r\sin\left(\frac{(1-k)d}{2r}\right)\right)^2 + 4rkd\sin\left(\frac{(1-k)d}{2r}\right)\cos\left(\frac{(1-k)d}{2r}\right)} \tag{2}$$

where k is the percentage of zipped length, d is the total length of the curved side, comprising both the zipped length a and unzipped length b, and r is the radius of curvature of curved sides. The overall kinematic of a single layer can be further derived as[17]

$$T = \begin{bmatrix} \cos(\gamma+\varepsilon) & -\sin(\gamma+\varepsilon) & 0 & 0 \\ \sin(\gamma+\varepsilon) & \cos(\gamma+\varepsilon) & 0 & 0 \\ 0 & 0 & 1 & l - \frac{4|\gamma+\varepsilon|}{\pi} \\ 0 & 0 & 0 & 1 \end{bmatrix} \tag{3}$$

In the matrix, the top left three-by-three matrix indicates the rotation along the z-axis, and the top left three-by-one matrix indicates the translation along the z-axis.

2.4. Fabrication of the OriZip Actuator

As shown in the explosive view of a single OriZip module in **Figure 3**A, the OriZip consists of two precurved insulated electrode layers connected to the input voltage. Each layer consists of two identical trapezoids connected at the leg, and each trapezoid is composed of three layers: the first layer is PVC tape (Advance AT7 with 0.13 mm thickness) at the interface between two electrodes. As an appropriate electrical insulator with a breakdown voltage of 8 kV,[29] it could effectively prevent the electrical breakdown between the electrode when they are energized; the second layer is a conductive copper film with a thickness of 0.1 mm; the third layer is two trapezoid shape precurved Mylar plastic film (RS PRO with the thickness of 0.075 mm) used as the backing material. As a thermoplastic material, the Mylar film can deform by the thermal treatment to program the curvature for elastic energy storage. Two insulated electrode layers are clamped to each other by two prezipping clamps, ensuring to partially cover the electrodes to initialize zipping actuation when the voltage is ON.

Each layer is cut into shape using a Cricut Maker with a fine point blade. Then, as shown in Figure 3B, it is inserted into the curve mold and heated in the curing oven at 70 °C for 60 min, aligning with the glass transition temperature of the Mylar which is 70 °C.[30] Both the mold and the prezipping clamp are fabricated by Anycubic Photon Mono SE SLA 3D Printer with Anycubic UV 405 nm Plant Based Photopolymer Resin. As shown in Figure 3C, two oven curved Mylar films are flattened onto the sticky board with their legs attached to each other. Subsequently, the copper film is adhered on top of the Mylar film, and conducting wires are also attached to the copper. To prevent leakage through the air gap between the PVC tape and Mylar film, and ensure durable attachment, super glue is applied to the edges, highlighted in red in Figure 3C, followed by sticking the PVC tape on top.

To assemble a single OriZip unit, as illustrated in Figure 3E, two electrodes are first prepared. These electrodes are then positioned with their PVC sides facing each other along the leg edge of trapezoid. Prezipping clamps are used to securely attach the electrodes at the edges. Once the electrodes are firmly clamped together, an eye dropper is employed to apply silicon oil into the clamped hinge area (labeled in red), serving as the dielectric liquid.

After fabricating eight OriZip modules, they are connected to each other by fishing wire through the holes on the zipping clamp located on the outer side, as shown in Figure 3F. Only two connection points are allowed on the outer side of the actuator between two adjacent OriZip units. Connecting them on the inner side would significantly restrict motion, as it would eliminate the interval, analyzed in Section 2.2, which ensures a full collapse.

2.5. OriZip Made of Flexible Printed Circuit Board

To speed up the fabrication process and minimize imperfections resulting from layer misalignments and copper thickness, which

© 2024 The Authors. Advanced Intelligent Systems published by Wiley-VCH GmbH

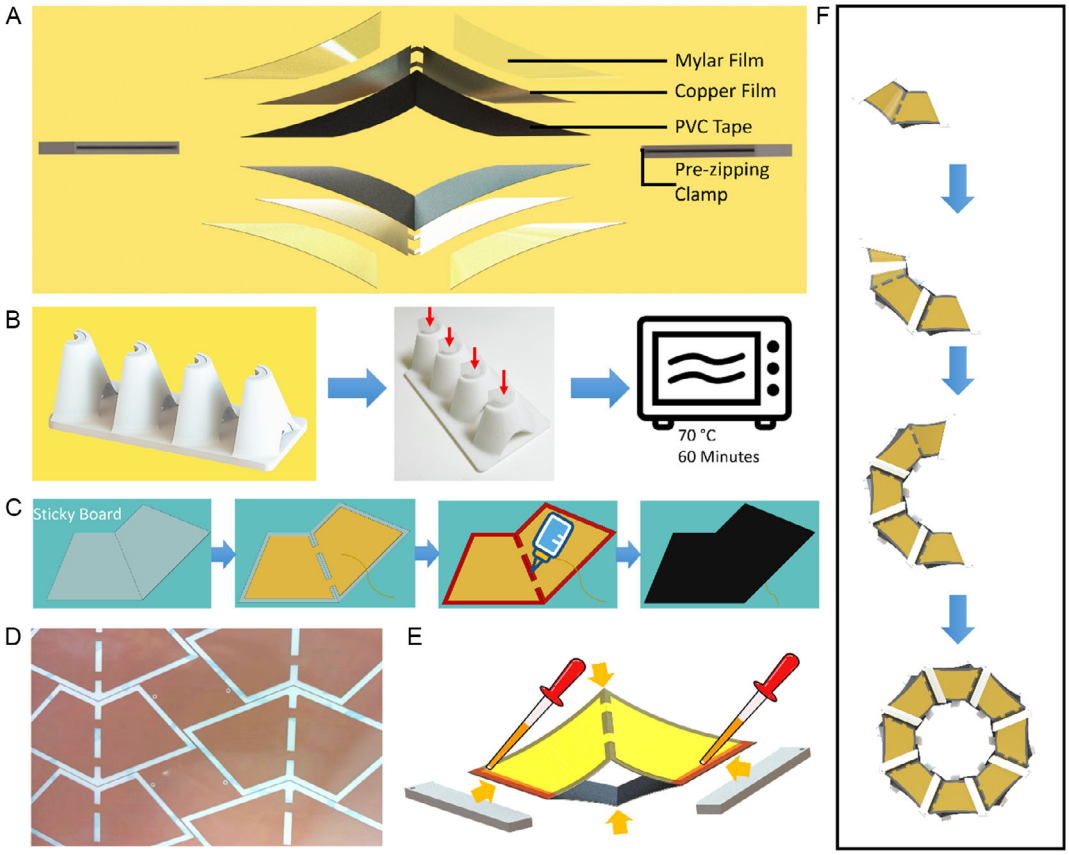


Figure 3. Fabrication of the electrozipping actuator. A) Explosive view of the OriZip actuator. B) The curve mold and the process of fabricating curved Mylar film as the backing material. C) The process of assembling a single electrode. D) The FPCB fabrication of the OriZip electrode. E) Illustration of the assembly of single OriZip unit and the application of dielectric liquid. F) Illustration of assembling eight OriZip units into a single-layer actuator by forming a circular pattern.

could potentially cause current leakage, we employed flexible printed circuit board (FPCB) technology to develop OriZip modules. This technology allows us to print precise patterns of ultrathin copper film on a polyethylene terephthalate (PET) substrate,[31] which is also a thermoplastic, with a PVC layer attached on top. The patterns shown in Figure 3D were printed on a 0.1 mm PET substrate using 0.1 mm copper film.

3. Results and Discussions

3.1. The Vertical Displacement and Twisted Angle

Twisting would always happen simultaneously with the tilting or shortening. **Figure 4**A,C shows the characterization of vertical displacement with laser displacement sensor, and Figure 4B,D shows the characterization of twisting angle with camera. The result of the characterization is shown in Figure 4E. The contraction, i.e., the percentage of the original height, increases with the actuation voltage and could reduce the height by an average of maximum 56.1% at 10 kV voltage, with the absolute value of the average height measured 11.9 mm at 10 kV. The measured twisted angle shows a very similar pattern, which increases from 1.5° at 3 kV to 5.4° at 10 kV. Both vertical displacement and twisted angle are smaller when compared to the theoretical model. The twisted angle could reach a maximum of 45°, and the height could reduce to the thickness of four electrodes at full collapse in the geometric model. One of the main reasons for this difference arises from the functioning principle of the DLZ, the attraction force between two parallel charged plates separated by insulator would exponentially decrease as the distance increases.[23] The electrostatic force significantly decreases as the distance increases, and thus creating a curved prefolding hinge with the clamp would significantly increase the initial zipping force. Introducing the clamp, however, results in the OriZip modules being shortened and twisted to a certain degree in their resting position. The clamp in OriZip units also limits their contraction capacity, preventing them from achieving complete collapse. The thickness of the prezipping clamps takes a large proportion of the final 11.9 mm height when the actuator has fully collapsed.

The standard deviation of both measurements is smaller at lower voltage, which indicates that the variance enlarges as the actuation voltage increases. We attribute it to the oil retention capability at different zipping positions. The presence of dielectric liquid, i.e., silicone oil here, is crucial to amplify the electrostatic force of the DLZ actuators at the hinge. At higher voltage, as the displacement increases, the curvature of the

© 2024 The Authors. Advanced Intelligent Systems published by Wiley-VCH GmbH

26404567, 2024, 6, Downloaded from https://advanced.onlinelibrary.wiley.com/doi/10.1002/aisy.202300738 by Imperial College London, Wiley Online Library on [23/06/2025]. See the Terms and Conditions (https://onlinelibrary.wiley.com/terms-and-conditions) on Wiley Online Library for rules of use; OA articles are governed by the applicable Creative Commons License

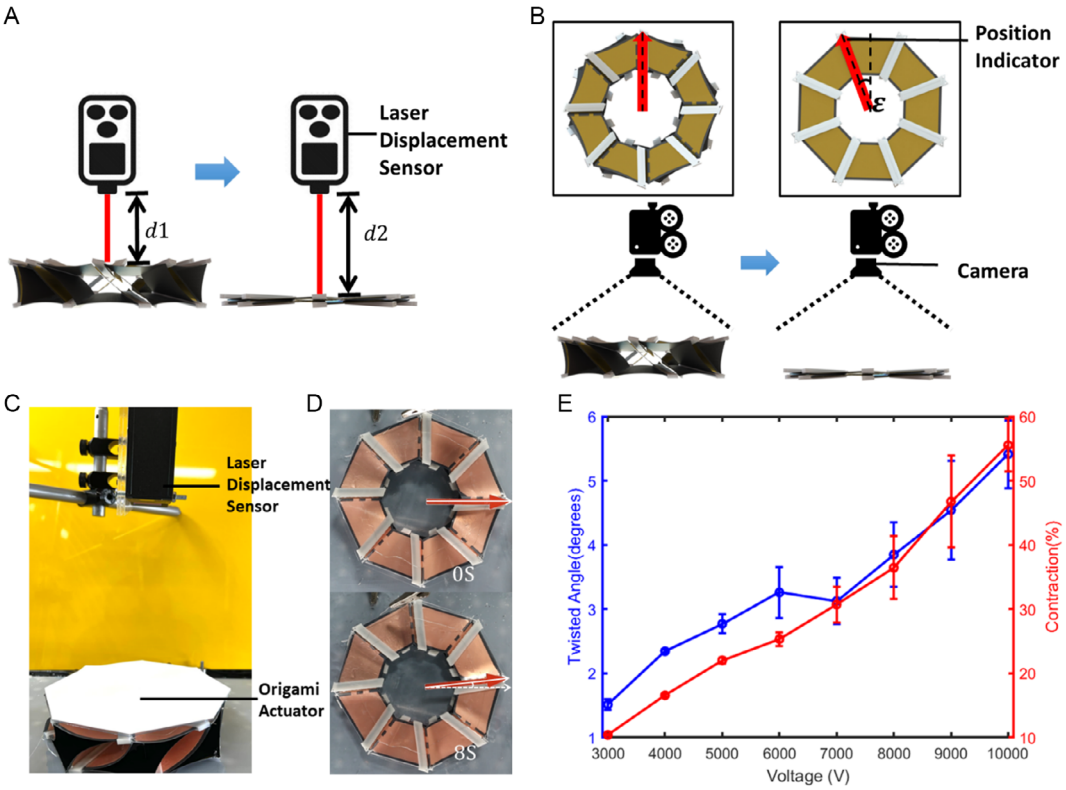


Figure 4. Vertical displacement and twisted angle experiments. A) The illustration of the setup for the veridical displacement experiment. B) The illustration of the setup for the twisting angle experiment. C) The image of the setup for the vertical displacement experiment. D) Snapshots of a typical twisted angle experiment. E) The relationship between the actuation voltage and maximum twisted angle (left *y*-axis labelled in blue), and vertical displacement (right *y*-axis labelled in red); the error bars represent the standard deviation of five trials.

OriZip could result in silicon oil to flow to the hinge on the hinge on the other side, which does not require zipping. For consistency in our characterization, we have applied the dielectric liquid to the zipping points prior to each test.

3.2. The Isometric Force Characterization

Figure 5 shows the isometric force characterization where one end of the actuator is fixed to the substrate and the other end is connected to the load cell. Three zipping positions are measured, including fully open (≈0 – 5% zipping), half open (≈50% zipping), and almost closed (≈95% zipping). The force measurement of different positions similarly shows a significant increase with the increase of voltage, with a very small variance in the results. Among the three positions, the almost closed position is capable of exerting the largest force, reaching 1.04 N at 10 kV, while the fully open position generated the lowest force with the maximum 0.78 N at 10 kV.

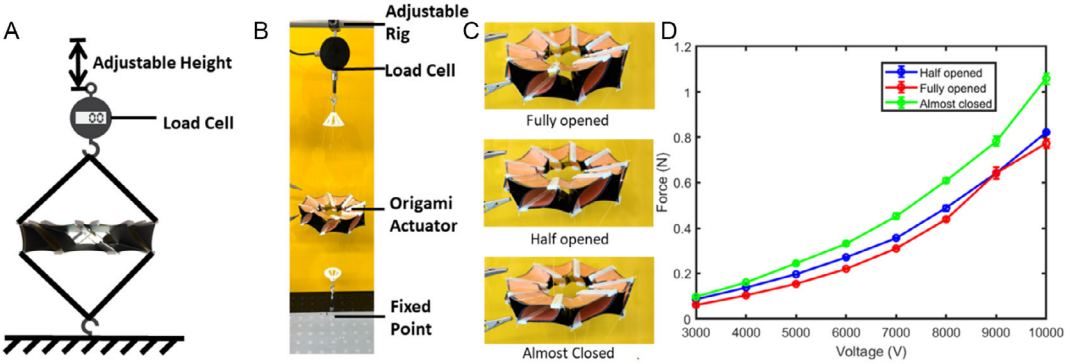


Figure 5. Isometric force experiment. A) The illustration of the setup of the isometric force experiment. B) The image of the setup for the isometric force experiment. C) The three force measuring positions. D) The relationship between the actuation voltage and maximum static force measured at different positions; the error bars represent the standard deviation of five trials.

© 2024 The Authors. Advanced Intelligent Systems published by Wiley-VCH GmbH

26404567, 2024, 6, Downloaded from https://advanced.onlinelibrary.wiley.com/doi/10.1002/aisy.202300738 by Imperial College London, Wiley Online Library on [23/06/2025]. See the Terms and Conditions (https://onlinelibrary.wiley.com/terms-and-conditions) on Wiley Online Library for rules of use; OA articles are governed by the applicable Creative Commons License

The curvature of the OriZip layers would act like a compression spring, which implies that at the fully opened position, a small force is required to compress it, and at the fully closed position, a large force is needed to overcome the elastic energy of the structure. In contrast, given that the zipping force is inversely proportional to the square of the distance between the electrodes,[24] and significantly increases as the distance gets closer, the zipping force is the largest when the zipping has almost reached a close position. This increased zipping force exerts a more pronounced influence when compared to the elastic force. Hence, the experimental result shows that the largest static force occurs at the almost closed position.

3.3. The Exerted Power and Power Efficiency

Figure 6 shows the isotonic characterization of the single-layer origami tower. The maximum mechanical power (gravitational potential power) and the maximum power efficiency of the actuator at different voltages are plotted in Figure 6C. The experimental section provides detailed information on the specific methodologies employed to plot these figures. As the voltage increases, the mechanical power exerted against gravity increases from 0.026 W at 6 kV to 0.106 W at 10 kV, and the variance of the measurement increases with voltage too. As the attached weight to the actuator is constant, this result implies that the maximum lifting velocity increases with the voltage. The power efficiency shows a reverse trend with the maximum at 64.7% when the mechanical power is minimal at 6 kV. When the voltage increases, the efficiency drops to 33.4% at 10 kV. This can be interpreted from the relationship between the average current and voltage, as shown in Figure S1, Supporting Information, the current increases almost linearly with voltage, while the change in peak velocity is relatively small compared to the product of the increasing voltage and current. This results in a decline in power efficiency at higher voltages. Given that the weight of the actuator is 38.2 g, the maximum mechanical power-to-weight ratio is calculated to be 2.775 W kg^{-1}, which is higher than other prebent DLZ configurations, such as the 1.59 W kg^{-1} of electrolattice actuator.[24] When considering both mechanical power and power efficiency, the optimal operation voltage is found to be 8 kV.

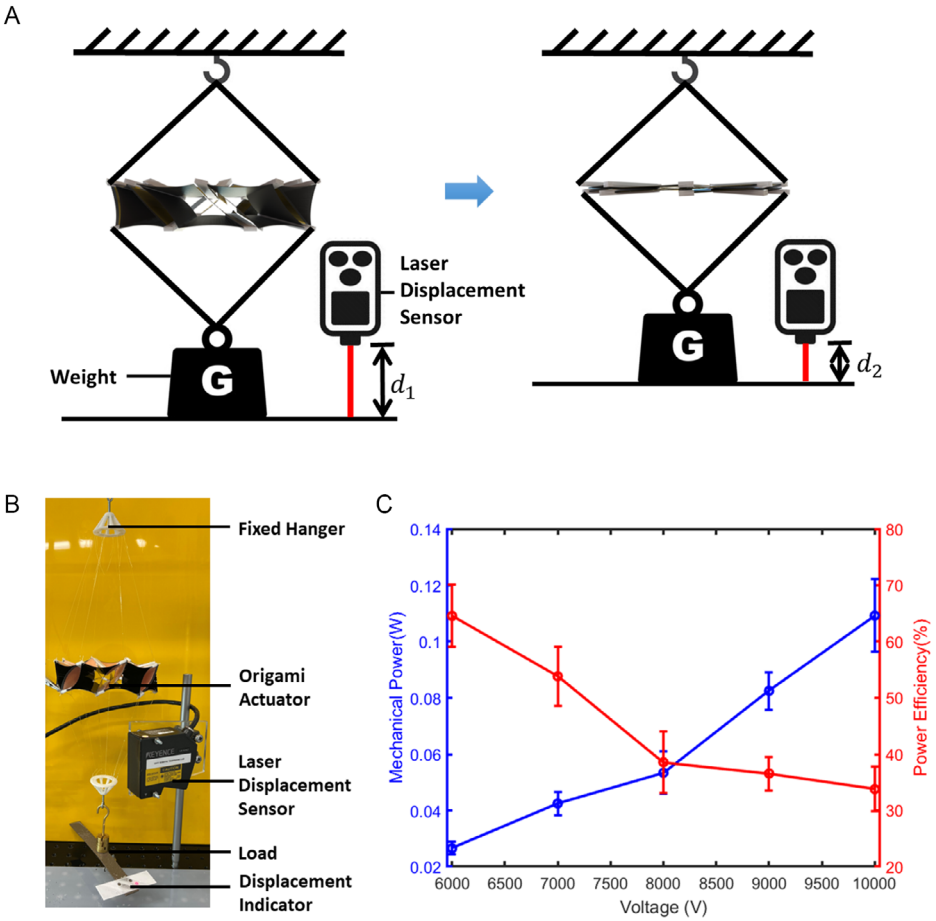


Figure 6. Dynamic loading experiment. A) The illustration of the setup for the dynamic loading experiment. B) The image of the setup for the dynamic loading experiment. C) The relationship between the actuation voltage and exerted maximum mechanical power (left *y*-axis labelled in blue), and maximum power efficiency (right *y*-axis labeled in red); the error bars represent the standard deviation of five trials.

© 2024 The Authors. Advanced Intelligent Systems published by Wiley-VCH GmbH

26404567, 2024, 6, Downloaded from https://advanced.onlinelibrary.wiley.com/doi/10.1002/aisy.202300738 by Imperial College London, Wiley Online Library on [23/06/2025]. See the Terms and Conditions (https://onlinelibrary.wiley.com/terms-and-conditions) on Wiley Online Library for rules of use; OA articles are governed by the applicable Creative Commons License

3.4. Multilayer and Wrist Motion Demonstration

The developed actuator can resemble human wrist motion, including flexion–extension, radial–ulnar deviation, and forearm supination–pronation. It can also shorten the arm, which occurs simultaneously with forearm supination–pronation (**Figure 7**B and Video S1, Supporting Information). Based on its actuation behavior, twisting always occurs concurrently with all these actuation modes. The effect is not significant when a single layer of the actuator is deployed (maximum of 5.4°), but it will be amplified when multiple layers are used to achieve a larger bending angle or shortening length (e.g., in a continuum arm architecture). The modular configuration of the proposed actuator allows us to cancel twisting when needed. It enables the development of wrist/arm actuators by stacking the origami tower layers in heterochiral and homochiral configurations (Figure 7A). The homochiral configuration, similar to traditional origami tower structure, generates layers of actuators with prezipping hinges aligned in similar directions, enabling maximum twisting and shortening. In contrast, heterochiral configuration, with prezipping hinges aligned in opposite directions, cancels out the twisting of one layer with the twisting of the other layer, allowing for bending of the structure when individual OriZip units on one side are actuated. Unlike homochiral or traditional origami tower structures that always twist in one direction, the heterochiral configuration can generate twisting motion in both directions when alternating layers are actuated. A schematic illustration of five pairs of actuators with opposite twisted directions is shown in

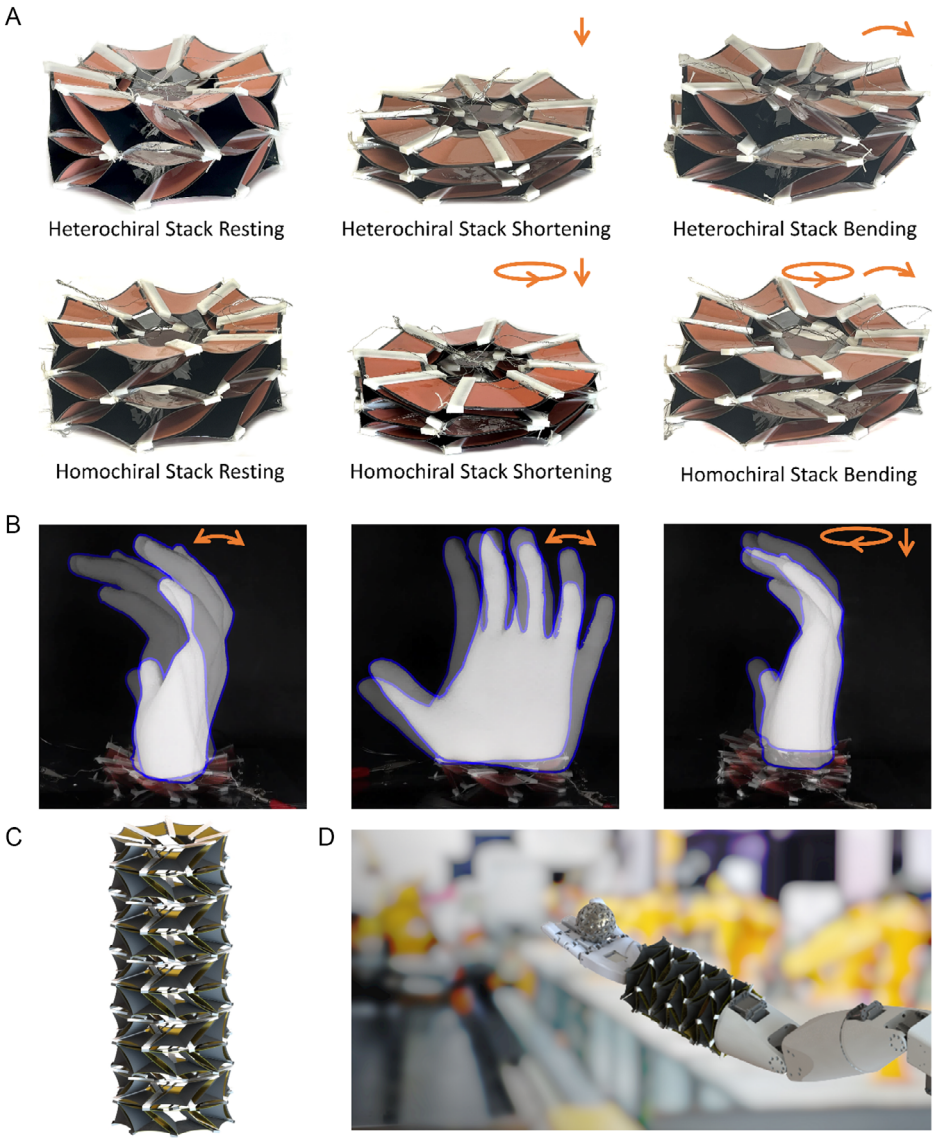


Figure 7. Demonstration of heterochiral and homochiral motion and potential applications. A) Demonstration of the differences in the resting state, shortening, and bending behaviors between heterochiral and homochiral configurations. B) The actuator with a model hand installed on top showing human wrist flexion–extension (left), radial–ulnar deviation (middle), pronation and supination (right). C) The rendering of stacking multiple layers on top of each other. D) The rendering of six layers of OriZip stacks as a robotic wrist to achieve higher DoF.

© 2024 The Authors. Advanced Intelligent Systems published by Wiley-VCH GmbH

26404567, 2024, 6, Downloaded from https://advanced.onlinelibrary.wiley.com/doi/10.1002/aisy.202300738 by Imperial College London, Wiley Online Library on [23/06/2025]. See the Terms and Conditions (https://onlinelibrary.wiley.com/terms-and-conditions) on Wiley Online Library for rules of use; OA articles are governed by the applicable Creative Commons License

26404567, 2024, 6, Downloaded from https://advanced.onlinelibrary.wiley.com/doi/10.1002/aisy.202300738 by Imperial College London, Wiley Online Library on [23/06/2025]. See the Terms and Conditions (https://onlinelibrary.wiley.com/terms-and-conditions) on Wiley Online Library for rules of use; OA articles are governed by the applicable Creative Commons License

Figure 7C that could potentially be employed as a multi-DoF robotic arm.

3.5. Limitations and Future Work

As discussed, the primary limitation of the design is that a significant proportion of the total displacement and twisting angle is consumed by the prezipping clamp, and the presence of rigid clamps increases the minimum actuated height of the structure. This limitation could be effectively addressed by introducing a larger curvature radius; however, this would also result in increased elastic force if the thickness of the backing Mylar film remains constant, leading to decreased exerted force. Therefore, future work will focus on studying the effect of the thickness of the backing material and its curvature on the generated displacement, twisting angle, and force. Additionally, the prezipping physical clamp could potentially be replaced with alternative physical and chemical bonding solutions to further increase the contraction.

Another limitation concerns the electrical connections, which become problematic at high voltage. DLZ actuators typically require a few thousand volts of actuation voltage. Despite their microscale current and energy levels, it increases the risk of electrical short-circuits between wires and breakdown through air. In our design, each layer has 16 electrodes that are required to be individually controlled to enable multi-DoF motion. This necessitates the use of thinner insulators with higher dielectric constants to decrease the operation voltage, not only ensuring safety in close-to-body applications but also compacting the operation electronics interface.

Furthermore, the performance of the actuator is influenced by the presence of dielectric liquid (silicone oil) at the hinge, which amplifies the electrostatic force required for contraction. To maintain cyclic stability, proper encapsulation of the silicone oil is crucial. During each actuation cycle, there is a tendency for some silicone oil to be expelled from the hinge, potentially diminishing performance in subsequent cycles due to the reduced presence of the dielectric liquid. Future investigation will include various encapsulation scenarios, including the use of oleophilic reservoirs in the origami structures or replacing silicon oil with ultrasoft gels to address this limitation.

The design complexity increases with the addition of layers to the structure. Depending on the testing configuration, the introduction of each layer imposes gravitational forces on others, impacting their displacement and force capacity. To tackle this, improving the electromechanical properties of the origami structure—such as using thinner insulator with a higher dielectric constant—and optimizing the stiffness of the structure, potentially through the integration of variable stiffness materials, can enhance the overall performance of multilayered origami structures.

4. Conclusion

A DLZ origami structure with multiple DoF, inspired by the "Twisted Tower" origami structure, has been developed. We developed a kinematic model of the actuator based on screw motion and demonstrated the feasibility of creating this structure using flexible PCB technology. A circular layer of OriZip elements is capable of achieving a maximum tilting of 3.9 degrees per layer along OriZip elements in multiple directions, a 56.1% contraction compared to the original length, a twisting of 5.4 degrees per layer, and each layer could generate a maximum of contractile force of 1.03 N. The power efficiency and power-to-weight ratio were found to be 64.7% and 2.775 $W\,kg^{-1}$, respectively. This study represents the initial steps toward the development of complex electrostatic-driven origami robots with a high degree of adaptability. It provides a practical solution for enabling multimodal motion in a wide range of robotic systems.

5. Experimental Section

The high voltage for actuation is provided by two Ultravolt HVA Series amplifiers that are controlled by National Instrument M Series DAQ. The software controlling data sampling, processing, and vitalization were conducted by MATLAB.

Vertical Displacement Experiment: The experiment is designed to determine the vertical displacement compared to the body length of the actuator at different actuation voltages. As shown in Figure 4A, a Keyence LK-G152 laser displacement sensor is placed above the actuator, with the laser vertically pointing downward on top of the actuator. A piece of paper is placed on top of the actuator to ensure a precise measurement of the overall displacement. For each trial, the voltage was turned ON for 10 s. The contraction $\varepsilon_{\text{contraction}}$ is determined by

$$\varepsilon_{\text{contraction}} = \frac{d_2 - d_1}{l} \tag{4}$$

where d_2 and d_1 are the final actuated and resting positions, respectively, and l is the height of the actuator at rest, which is 27 mm.

Twisting Angle and Tilting Angle Experiment: As shown in Figure 4B, a camera is installed with the lens vertically pointing downward right above the actuator. A transparent plate is fixed on top of the actuator with a red arrow function as a position indicator. The voltage was turned ON for 10 s while the camera kept recording the position of the red arrow. Then the recorded video is imported into the MATLAB App DLTdv8a to estimate the angle formed by the vector of initial indicator pixel positions and the final pixel positions.

The 3.9 degree tilting angle measurement was obtained through similar method, which included manual labeling and measurement from photographs (Figure 1E), captured with a camera positioned alongside the actuator.

Isometric Force Experiment: The isometric force experiment is designed to determine the static force of the actuator at different zipping positions. The experimental setup is shown in Figure 5A, where a Richmond Industries 900 series 5 N load cell with Strain Gauge Amplifier AMP3 is connected to an adjustable test rig. The load cell is linked to the actuator, while the bottom of the actuator is fixed to the floor. The height of the adjustable test rig has been set at various levels to measure the associated isometric zipping force. The voltage was turned ON for 10 s and then turned OFF while the force was recorded. To eliminate the effect of gravity, the final maximum force is calculated by subtracting the initial unactuated force from the final static force.

Dynamic Loading Experiment: The exerted mechanical power and the power efficiency are determined by the dynamic loading experiment. A fixed weight was lifted by the actuator, and the voltage was turned ON for 30 s before being turned OFF while the motion of the weight was tracked by the laser displacement sensor throughout the lifting (Figure 6A). The mechanical power during the lifting is estimated as the gravitational potential power:

$$P_{\text{mech}} = Fv = mg\frac{d_2 - d_1}{dt} \tag{5}$$

© 2024 The Authors. Advanced Intelligent Systems published by Wiley-VCH GmbH

where $d_2 - d_1$ represents the change in position of the weight during the time interval, dt is the length of the time interval, m is the mass of the weight (76.6 g in this case), and g is the gravitational constant. The electrical power consumption is estimated by

$$P_{elec} = VI \tag{6}$$

And the peak efficiency of the actuator is calculated by

$$\eta_{max} = \max\left(\frac{P_{mech}}{P_{elec}}\right) \tag{7}$$

The raw measurement data of displacement were noisy due to the instability of the hanged indicator for the laser displacement sensor. To avoid affecting velocity calculation, a Gaussian window with a size of 100 was applied to smooth the data. Afterward, the data were sampled at a rate of 100 Hz to further reduce the noise before calculating the power.

Supporting Information

Supporting Information is available from the Wiley Online Library or from the author.

Acknowledgements

This work was supported by the M. T. acknowledges Imperial College Fellowship.

Conflict of Interest

The authors declare no conflict of interest.

Data Availability Statement

Data supporting this study are openly availiable from Zenodo at https://doi.org/10.5281/zenodo.10842437.

Keywords

dielectrophoretic liquid zipping, electro-ribbon, modular, multi-degrees of freedom, origami

Received: November 8, 2023
Revised: February 19, 2024
Published online: April 8, 2024

[1] C. Zhang, Z. Zhang, Y. Peng, Y. Zhang, S. An, Y. Wang, Z. Zhai, Y. Xu, H. Jiang, *Nat. Commun.* **2023**, *14*, 4329.
[2] H. Fan, G. Wei, L. Ren, *Robotica* **2022**, *40*, 4169.
[3] W. Yue, J. Qi, X. Song, S. Fan, G. Fortino, C. H. Chen, C. Xu, H. Ren, *Sensors* **2022**, *22*, 5370.
[4] M. A. Robertson, O. C. Kara, J. Paik, *Int. J. Rob. Res.* **2020**, *40*, 72.
[5] Origami - History of Origami | Britannica, https://www.britannica.com/art/origami/History-of-origami (accessed: September 2022).
[6] D. Rus, M. T. Tolley, *Nat. Rev. Mater.* **2018**, *3*, 101.
[7] C. H. Belke, J. Paik, *IEEE/ASME Trans. Mechatron.* **2017**, *22*, 2153.
[8] S. P. Murali Babu, R. Das, B. Mazzolai, A. Rafsanjani, in *2023 IEEE Int. Conf. Soft Robotics (RoboSoft)*, IEEE, Piscataway, NJ **2023**.
[9] T. Amadeo, D. Van Lewen, T. Janke, T. Ranzani, A. Devaiah, U. Upadhyay, S. Russo, *Front. Rob. AI* **2022**, *8*, 731010.
[10] D. Tang, C. Zhang, H. Sun, H. Dai, J. Xie, J. Fu, P. Zhao, *Nano Energy* **2021**, *89*, 106424.
[11] S. Wu, Q. Ze, J. Dai, N. Udipi, G. H. Paulino, R. Zhao, *Proc. Natl. Acad. Sci.* **2021**, *118*, e2110023118.
[12] S. Miyashita, S. Guitron, M. Ludersdorfer, C. R. Sung, D. Rus, in *2015 IEEE Int. Conf. Robotics and Automation (ICRA)*, IEEE, Piscataway, NJ **2015**.
[13] S. Wu, Q. Ze, J. Dai, N. Udipi, G. H. Paulino, R. Zhao, *Proc. Natl. Acad. Sci.* **2021**, *118*, e2110023118.
[14] R. V. Martinez, C. R. Fish, X. Chen, G. M. Whitesides, *Adv. Funct. Mater.* **2012**, *22*, 1376.
[15] C. De Pascali, G. A. Naselli, S. Palagi, R. B. Scharff, B. Mazzolai, *Sci. Rob.* **2022**, *7*, eabn4155.
[16] K. Zhang, Y. Zhu, C. Lou, P. Zheng, M. Kovac, in *2019 2nd IEEE Int. Conf. Soft Robotics (RoboSoft)*, IEEE, Piscataway, NJ **2019**.
[17] J.-G. Lee, H. Rodrigue, *Soft Rob.* **2019**, *6*, 109.
[18] L. Paez, G. Agarwal, J. Paik, *Soft Rob.* **2016**, *3*, 109.
[19] H. Banerjee, N. Pusalkar, H. Ren, *J. Mech. Rob.* **2018**, *10*, 064501.
[20] E. Vander Hoff, D. Jeong, K. Lee, in *2014 IEEE/RSJ Int. Conf. Intelligent Robots and Systems*, IEEE, Piscataway, NJ **2014**.
[21] P. Velvaluri, A. Soor, P. Plucinsky, R. L. de Miranda, R. D. James, E. Quandt, *Sci. Rep.* **2021**, *11*, 10988.
[22] Shape Memory Alloy, https://www.sciencedirect.com/topics/engineering/shape-memory-alloy (accessed: September 2022).
[23] P. Boyraz, G. Runge, A. Raatz, *Actuators* **2018**, *7*, 48.
[24] M. Taghavi, T. Helps, J. Rossiter, *Sci. Rob.* **2018**, *3*, eaau9795.
[25] S. Hoh, T. Helps, R. S. Diteesawat, M. Taghavi, J. Rossiter, *Smart Mater. Struct.* **2021**, *30*, 125034.
[26] M. Taghavi, T. Helps, J. Rossiter, in *2020 IEEE Int. Conf. Robotics and Automation (ICRA)*, IEEE, Piscataway, NJ **2020**.
[27] R. S. Diteesawat, A. Fishman, T. Helps, M. Taghavi, J. Rossiter, *Front. Rob. AI* **2020**, *7*, 557624.
[28] Twisted Tower - Mihoko tachibana: Paper Art, Origami, Paper, Pinterest, https://www.pinterest.com/pin/twisted-tower-mihoko-tachibana--234187249344514430/ (accessed: September 2022).
[29] AT7 PVC Electrical Insulation Tape, https://docs.rs-online.com/fdd0/0900766b8157ce6b.pdf (accessed: September 2022).
[30] J. P. Jog, *J. Macromol. Sci., Part C: Polym. Rev.* **1995**, *35*, 531.
[31] Ipcb, PCB, https://www.ipcb.com/technical/7437.html#:~:text=The%20FPCB%20is%20a%20cover,PI)%2C%20are%20commonly%20used (accessed: September 2022).

© 2024 The Authors. Advanced Intelligent Systems published by Wiley-VCH GmbH

26404567, 2024, 6, Downloaded from https://advanced.onlinelibrary.wiley.com/doi/10.1002/aisy.202300738 by Imperial College London, Wiley Online Library on [23/06/2025]. See the Terms and Conditions (https://onlinelibrary.wiley.com/terms-and-conditions) on Wiley Online Library for rules of use; OA articles are governed by the applicable Creative Commons License